ADVANCED ENERGY MATERIALS
www.advenergymat.de

An Aqueous Sodium Ion Hybrid Battery Incorporating an Organic Compound and a Prussian Blue Derivative

Dong Jun Kim, Young Hwa Jung, K. Kamala Bharathi, Sang Hyun Je, Do Kyung Kim, Ali Coskun,* and Jang Wook Choi**

Rechargeable batteries are currently encountering a new demand for emerging applications, so-called grid-scale energy storage systems (ESSs).[1] In particular, development of ESSs are especially meaningful as they are expected to play crucial roles in resolving various energy and environmental issues on the global scale. They could serve as storage systems for efficient distribution of the electricity generated from renewable resources, such as sunlight and wind.

The rechargeable batteries used for grid-scale ESSs require distinctive standards compared to those for conventional LIBs.[2] Above all, the batteries should be made from cheap and abundant raw materials for economic viability. The cells should also warrant long cycle life (one or two orders of magnitude longer than those of the current LIBs), good rate performance, and safety, but the energy density may be compromised to a certain level for the aforementioned aspects. With these standards, sodium ion batteries (SIBs) with decent electrochemical performance might be more suitable than the existing LIBs because sodium raw materials are much cheaper (30–40 times), and their reserves are more abundant and locationally flexible.[3] Moreover, operation of SIBs in aqueous electrolytes may be more preferred than those in conventional organic electrolytes in the safety and cost perspectives.[4–6] Aqueous electrolytes also allow for higher ionic motilities and can thus compensate relatively sluggish kinetics of SIBs. However, use of aqueous electrolytes impose a significant challenge in finding appropriate anode and cathode materials that operate within the limited potential window of water while generating reasonably large cell-voltages.[7,8] Until now, finding suitable anode materials for aqueous electrolytes appeared to be more difficult[9] because most transition metals within common crystal frameworks position their redox potentials too high for the aqueous anodes. Also, the redox potentials of most anodes studied[10] in organic electrolyte cells are too low. Therefore, new approaches are needed for development of high performance anode materials suitable for aqueous electrolytes and, as a result of such research trend, polymeric materials were recently investigated.[6]

Various designs and approaches have been introduced recently to use redox active organic compounds as active electrode materials for rechargeable batteries.[11,12] The recent discovery of organic SIB anodes for organic electrolytes is a good example along this direction.[13,14] Also, in-depth analysis of these organic materials allow one to understand structural effects on the cell performance.[15–17] For the case of naphthalenediimide (NDI), we have previously demonstrated the critical effect of the substitution at the *N*-site of NDI on the battery performance,[18] which allowed us to utilize this concept in the making of electrodes for the present aqueous SIBs.

Here, we report a new carbonyl-based organic salt, namely disodium naphthalenediimide (SNDI) (**Figure 1**a), as an aqueous SIB anode with a well-defined redox plateau at –0.14 V versus standard hydrogen electrode (SHE). Remarkably, this voltage value is the lowest reported to date among those showing single-valued plateaus within the stable water potential window. Furthermore, we paired SNDI with one of the Prussian blue (PB) derivatives as a cathode, $KCo_{0.5}Cu_{0.5}Fe(CN)_6$, thus forming, for the first time, a hybrid aqueous full-cell made up of cheap electrode materials that can be synthesized using very simple procedures at low temperatures (<100 °C). The good electrochemical performance of this new battery setting suggests that aqueous cells employing cheap unconventional electrode materials can offer a feasible alternative for grid-scale ESSs.

SNDI was synthesized (Figure 1a) by a simple two-step reaction. 1,4,5,8-naphthalenetetracarboxylic dianhydride was reacted[19] with concentrated ammonium hydroxide solution under N_2 atmosphere in order to form 1,4,5,8-naphthalenetetracarboxylicdimide (HNDI), which was subsequently treated with sodium hydride (NaH) in anhydrous dimethylformamide (DMF) for 16 h to yield SNDI as a yellow powder. The product was annealed at 200 °C for 1 h in order to remove both remaining and coordinating solvent molecules.

Formation of SNDI was confirmed by elemental analysis (EA) and ^{1}H-NMR spectroscopy (Supporting Information, Figure S1). The disappearance of imide protons along with a

D. J. Kim, Y. H. Jung, K. K. Bharathi, Prof. D. K. Kim
Department of Materials Science and Engineering
Korea Advanced Institute of Science and Technology (KAIST)
291 Daehak-ro, Yuseong-gu, Daejeon 305–701, Republic of Korea
E-mail: dkkim@kaist.ac.kr
S. H. Je, Prof. A. Coskun, Prof. J. W. Choi
Graduate School of Energy
Environmental Water and Sustainability
Korea Advanced Institute of Science and Technology (KAIST)
291 Daehak-ro, Yuseong-gu, Daejeon 305–701, Republic of Korea
E-mail: coskun@kaist.ac.kr; jangwookchoi@kaist.ac.kr
Prof. J. W. Choi
Center for Nature-inspired Technology (CNiT)
KAIST Institute NanoCentury
Korea Advanced Institute of Science and Technology (KAIST)
291 Daehak-ro, Yuseong-gu, Daejeon 305–701, Republic of Korea

DOI: 10.1002/aenm.201400133

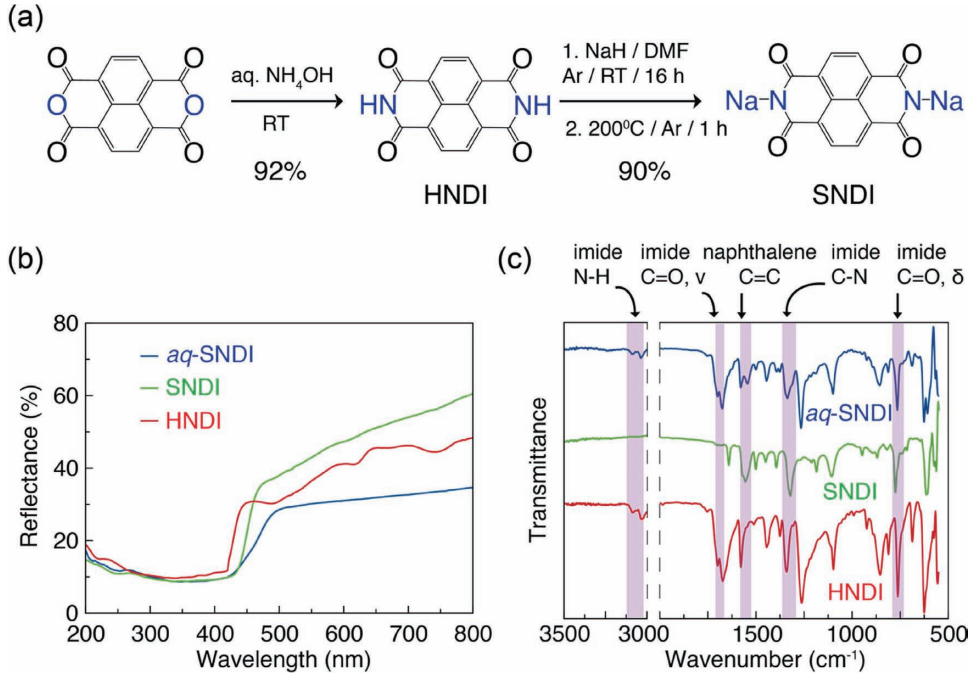

Figure 1. a) A synthetic route for production of disodium naphthalene diimide (SNDI). b) UV-vis and c) FTIR spectra of HNDI, SNDI, and *aq*-SNDI.

down field shift of aromatic protons clearly indicates quantitative conversion of HNDI into SNDI. In addition, experimental EA data (Supporting Information) are also in perfect agreement with the theoretical data, thus further confirming the formation and the purity of SNDI. Furthermore, we have also carried out UV-vis (Figure 1b) and Fourier transform infrared (FTIR) (Figure 1c) spectroscopic analyses to verify the formation of series of NDIs, namely HNDI, SNDI, and *aq*-SNDI (SNDI immersed in the aqueous electrolyte), and also to investigate stability of SNDI in an aqueous electrolyte. Notably, the persistent UV-vis spectra of all of the three samples confirmed that there are no side reactions such as hydrolysis upon immersion of SNDI (Figure 1b) into an aqueous electrolyte. A small blue shift in the reflectance spectrum of *aq*-SNDI suggests partial protonation of SNDI. The FTIR spectra of all of the three samples commonly showed the characteristic absorption bands at 1570, 1348, 765, 1680, and 3000–3200 cm^{-1} corresponding to the naphthalene C=C stretching, imide C–N vibration, imide $C{=}O_{\delta}$ bending, imide C=O vibration, and imide N–H stretching, respectively, of the NDI moiety.[20] However, the FTIR spectrum of *aq*-SNDI showed absorption bands associated with both HNDI and SNDI even before any battery operations, indicating that the exposure of SNDI to the aqueous electrolyte immediately promoted partial protonation, (H)SNDI. In addition, (H)SNDI turned out to be insoluble in the aqueous electrolyte, as the UV-vis spectrum of the electrolyte solution containing (H)SNDI did not show any signals.

Electrochemical characterization of (H)SNDI was performed by employing cyclic voltammetry (CV) and galvanostatic measurements in a three-electrode flooded beaker cell. Hereafter, all of potentials are noted with respect to SHE. The CV data (**Figure 2**a) indicated that (H)SNDI undergoes reversible redox reactions at potentials around –0.15 V.

In the first cycle, (H)SNDI exhibited reduction and oxidation peaks at –0.37 V and 0 V, respectively. In the second cycle, the reduction peak was shifted to –0.3 V, while the oxidation peak remained at the same potential. From the CV data, it is anticipated that certain stabilization processes took place at the electrode-electrolyte interface during the first reduction. Upon stabilization of the interface, the redox peaks remained preserved from the first oxidation through subsequent cycles. The reversible peaks in the CV profiles are the first indication of the reversible and robust character of (H)SNDI during its reaction with Na ions in an aqueous environment. Since Na metal is not stable in water, the galvanostatic tests were performed by employing an excessively large size of partially discharged (sodiated) (H)SNDI as a counter electrode. The galvanostatic profiles of (H)SNDI showed well-defined single discharge (sodiation) and charge (desodiation) plateaus at –0.25 V and –0.03 V, respectively, which are in a good agreement with the CV data. At a 6C rate, (H)SNDI exhibited a reversible capacity of 62 mAh g^{-1}. This capacity indicates that 0.7 Na ion binds reversibly with each formula unit of SNDI, which is quite unexpected when compared to naphthalenedimide dilithium case, where 1.5 Li ions bind reversibly.[18] The C-rate was defined such that 1C corresponds to 86 mA g^{-1} based on the theoretical capacity when one Na ions bind with each (H)SNDI molecule. In addition, all of the C-rates reported in this study are based on the current density with respect to 1C, not actual charge or discharge durations.

When tested at various C-rates, (H)SNDI showed good rate performance. Even when the C-rate was increased from 6C to 24C, a specific capacity of 40 mAh g^{-1} was still preserved, which corresponds to 60% capacity retention. Although polypyrrole-carbon composite electrodes were demonstrated as anode materials for potassium ion batteries in aqueous electrolytes,[21]

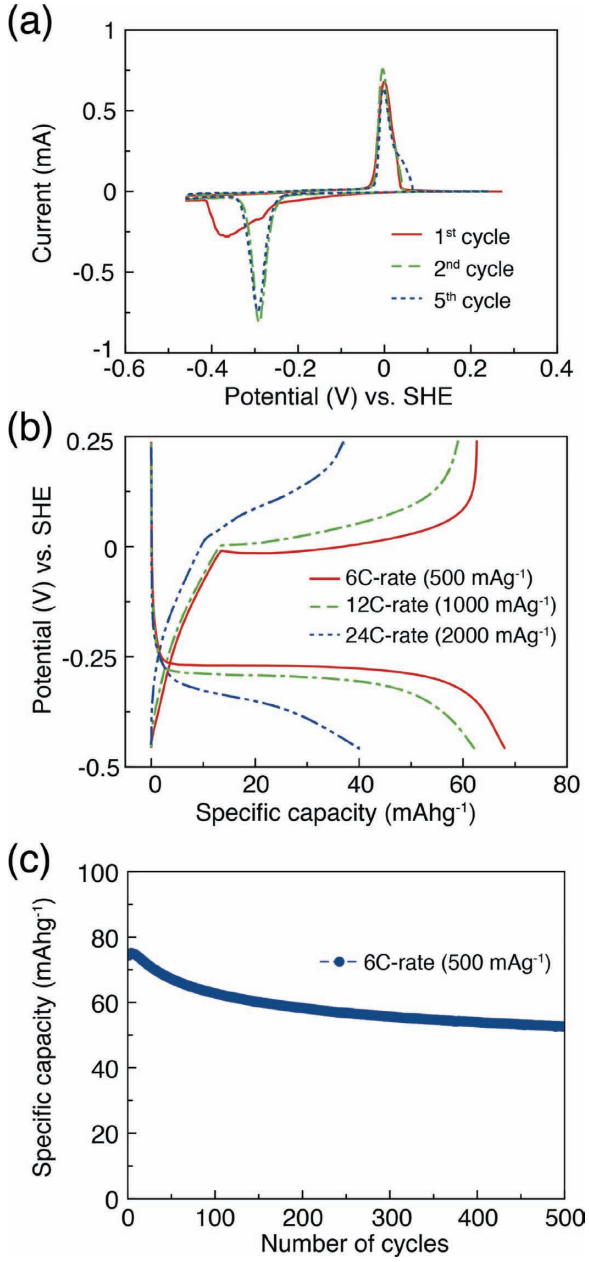

Figure 2. a) Cyclic voltammetry scans of (H)SNDI at different cycle numbers. The scan rate was 400 μV s^{-1}, and the voltage range was –0.46–0.24 V vs. SHE. b) Galvanostatic voltage profiles of (H)SNDI half-cells measured at different C-rates. c) Discharging cycling performance of (H)SNDI measured at 6C. The C-rates were the same for charge and discharge in each cycle. 1C = 86 mA g^{-1}.

(H)SNDI is substantially distinctive since it exhibits well-defined flat voltage plateaus. On the contrary, the polypyrrole-based electrodes exhibited[21] sloping voltage profiles with serious steepness and thus require excessive loading of the active materials for well-defined voltages over a good portion of the state of charge in full-cell operations. In addition, the robust reversible reaction of (H)SNDI with Na ions translated into a stable cycle life in the extended cycling period. As shown in Figure 2c, 53 mAh g^{-1} was preserved at the end of 500 cycles, corresponding to 74% capacity retention. We have further investigated high temperature cycling performance of (H)SNDI (Supporting Information, Figure S2a) and observed reasonably stable capacity retention: after 100 cycles, the capacity retentions were 86% and 66% at room temperature and 60 °C, respectively, when measured at 6C. Interestingly, we observed that, at 6C, the initial capacity at 60 °C was higher than that at room temperature by ≈5%, which might be due to increased mobility of Na ions at the elevated temperature. Also we have carried out (Supporting Information, Figure S2b) galvanostatic tests on HNDI in the same aqueous electrolyte. Remarkably, we observed a serious capacity decay (27% retention) after 150 cycles, indicating the fact that the presence of Na ions at the *N*-sites of naphthalenedimide is crucial for the stability of the electrode.[18] In addition, the partial protonation of SNDI to (H)SNDI does not alter the stability of the electrode material.

The reversible nature of (H)SNDI during electrochemical reactions was further verified using FTIR, X-ray diffraction (XRD), and electron paramagnetic resonance spectroscopy (EPR). All of the measurements were performed after the galvanostatic pre-cycling, and we refer to the sample after the pre-cycling as "as-prepared". Although moderate peak-shifts and intensity changes were observed due to the altered bond characters upon sodiation, the FTIR spectra (**Figure 3**a) before and after a full cycle were quite similar, implying the reversible structural changes over a complete cycle. Upon sodiation, it was observed that the N–H band at 3000–3200 cm^{-1} disappeared and the O–H band at 3300 cm^{-1} newly appeared, from which we propose a reaction mechanism, where amide tautomerization occurs in order to stabilize the sodiated-state (Supporting Information, Figure S3). The XRD analyses at the same electrochemical states further confirm (Figure 3b) the reversible nature of (H)SNDI. The XRD spectrum of the as-prepared state showed peaks at $2\theta = 15°$ and 21°, which are in good agreement with the report by Ahmed et al.,[22] suggesting that NDI holds monoclinic structure with extended π–π stacking. Upon full sodiation, the intensities of both major peaks decreased, which is attributed to the weakened π–π stacking interactions by Na ion insertion and lowered crystallinity. However, upon full desodiation, the intensities of those peaks were fully recovered to the levels of the as-prepared state. In addition, inductively coupled plasma mass spectroscopy (ICP-MS) was used to attain the Na ratio between the sodiated and desodiated states. The Na ratio between both states turned out to be 2.25, which is reasonably close to the designated value of 2. The ex situ characterizations of FTIR and XRD were also obtained for HNDI (Supporting Information, Figure S4). Unlike (H)SNDI, the FTIR spectrum of HDNI showed an N-H band around 3000–3200 cm^{-1} in the sodiated state, implying that HNDI undergoes tautomerization only around the N-site near the oxygen where Na ion binds, but leaves the N-H bond at the opposite N-site. The XRD result of HNDI also showed a bit different behavior upon sodiation (red mark in Figure S4b). More critically, after 50 cycles, it was observed (Figure S4c) that a large portion of the HNDI electrode peeled off as tiny particles, which is in sharp contrast to the (H)SNDI electrode prepared and measured at the same conditions. It is anticipated that the distinct phase transformation of HDNI during (de)sodiation affects the mechanical stability of its electrode film and thus cycling performance. Overall, the different

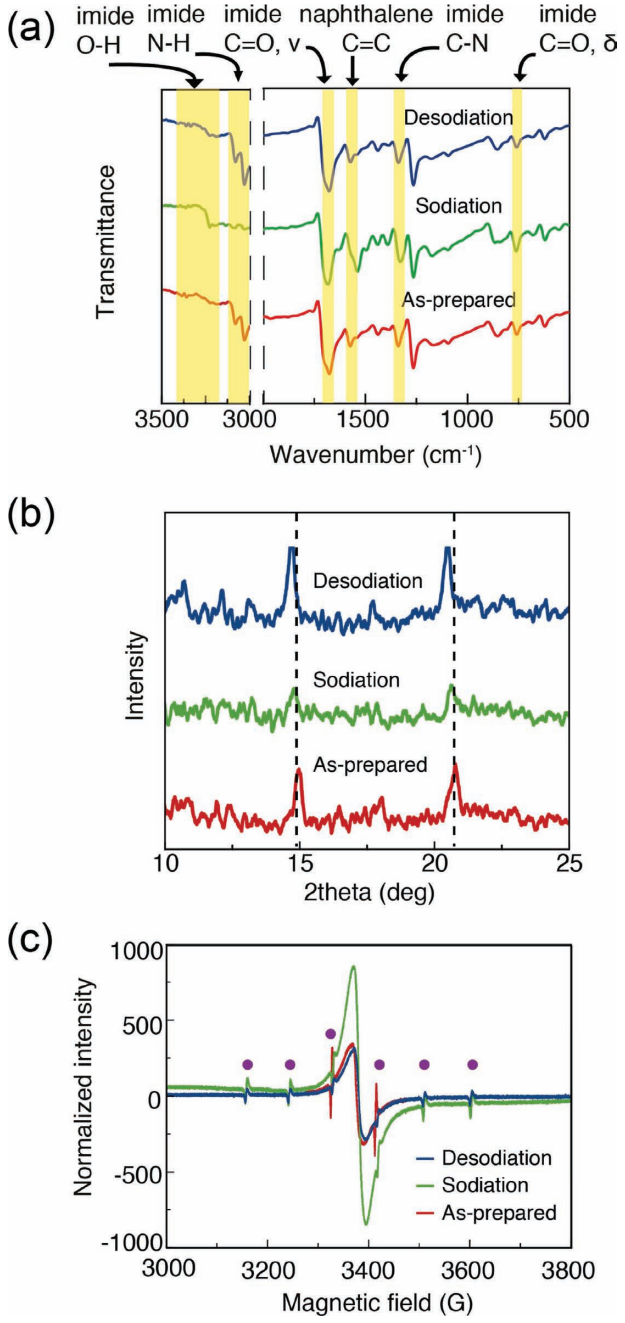

Figure 3. Ex-situ characterizations of (H)SNDI at the as-prepared, fully sodiated (sodiation, –0.46 V), and fully desodiated (desodiation, +0.24 V) states: a) FTIR, b) XRD, and c) EPR measurements. In (c), the purple dots correspond to the Mn reference and were used for calculation of the Landė *g* factor (*g*).

characterization results and cell performance reconfirm the importance of N-substitution in this class of organic molecules, which is consistent with other previous reports.[18,23,24]

In order to verify the insertion of Na ions, we have carried out EPR analyses on (H)SNDI. The Gaussian shape lines shown in the EPR spectra (Figure 3c) confirm that, under the magnetic fields, there indeed exist the split energy levels for all of the three states of SNDI. Also, the Landė *g* values turned out to be 1.99 in all of the three states (see Supporting Information, Equation S1), which indicates the spin quantum number of $S = ½$ and thus verifies the presence of the unpaired electron spins in all of the three states. In the sequential EPR profiles, the EPR peaks were enhanced at the sodiation state but were lessened back to the as-prepared level after a full redox cycle, reconfirming robust reversibility of (H)SNDI through the radical-anion form at the sodiation state.[25] In addition, it is noteworthy that the as-prepared and desodiated samples still exhibited small EPR peaks due to presence of the (H)SNDI molecules under the residual radical-anion forms from the previous cycles, as previously observed in a similar case.[26]

Recently, Cui et al.[21,27–30] reported the use of PB derivatives as cathode materials for aqueous rechargeable batteries. The large continuous ionic channels present in the crystal structures of these materials facilitate efficient diffusion of various carrier ions (Li^+, Na^+, K^+, etc.), enabling excellent rate performance and long-term cyclability.[28,29] However, it should be noted that all of these PB derivatives were tested in highly acidic conditions because the redox operating voltages of K^+ (de)intercalation with those PB derivatives are above the stable potential window of neutral water. However, the use of acidic electrolytes is not desirable for grid-scale applications in the safety and processing perspectives. In an effort to use electrolytes at neutral pHs, we have replaced a good portion of Fe in the conventional ferric ferrocyanides with cobalt (Co) and copper (Cu), as inclusion of these transition metals positions the redox operating voltage of the PB derivative almost to the highest value within the stable water potential window at neutral conditions while delivering excellent cycle life. Although the use of Co could increase the material cost in the cell production, the safety is also critical for large-scale cells. Thus, the material cost may have to be sacrificed to some extent in the current system. For reference, the PB derivative where a good portion of Fe is replaced by Ni exhibited a lower redox voltage of 0.56 V (Supporting Information, Figure S5). Also, the PB derivative where Fe is replaced only by Cu showed inferior cycling performance (Supporting Information, Figure S6). Based on these results, $KCo_{0.5}Cu_{0.5}Fe(CN)_6$, or shortly CoCuHCF, that exhibits average redox potential at 0.9 V vs. SHE was selected in the current investigation and synthesized by a simple precipitation process (see Supporting Information for details). The XRD spectrum (**Figure 4**a) of CoCuHCF was in good agreement with the previously reported[31] PB derivatives and thus indicates the proper crystal structure of the synthesized CoCuHCF. Although CoCuHCF has been explored[32] for hydrazine ion screening since the early 2000s, to the best of our knowledge, this material has never been investigated for battery electrodes.

Galvanostatic voltage profiles of CoCuHCF (Figure 4b) measured at 10C (500 mA g^{-1}) showed clear redox activity in the potential range of 0.7–1.1 V and a reversible capacity of 39 mAh g^{-1}. In this Na half-cell configuration, potassium ions are extracted in the first charge and subsequently Na ions are (de)inserted in the first discharge and in the following cycles. Similar to the previous PB derivatives,[29] CoCuHCF showed excellent electrochemical performance. As shown in Figure 4c, after 200 cycles, 95% (=500 mA g^{-1}) of the initial capacity was retained and Coulombic efficiency reached 99.2%, reconfirming robust diffusion of Na ions through the well-developed

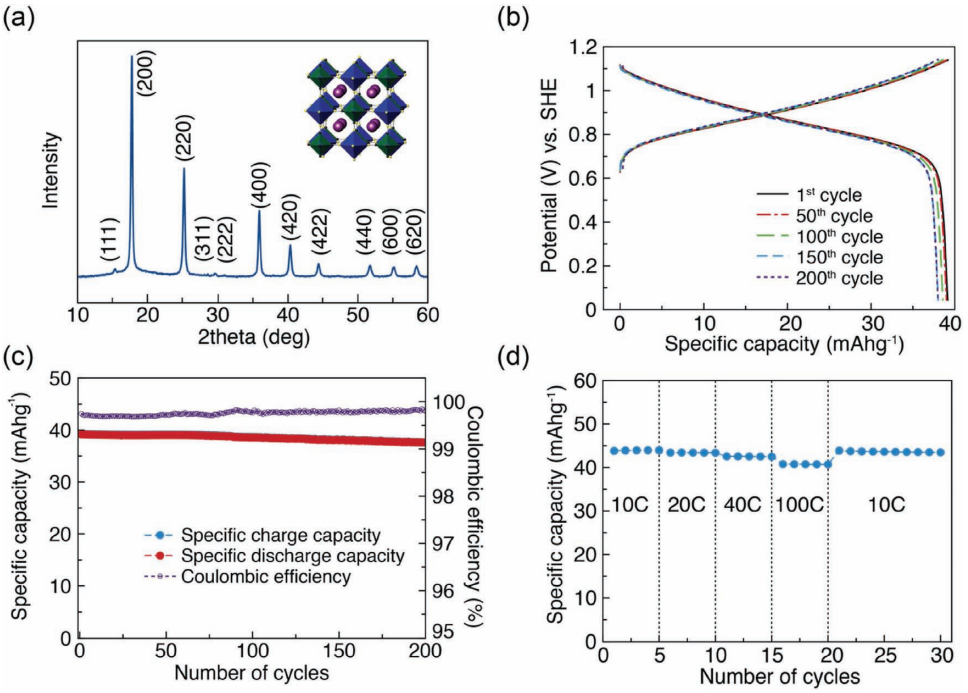

Figure 4. a) The XRD spectrum of CoCuHCF and its corresponding lattice orientation to each peak. b) The galvanostatic profiles of the CoCuHCF half-cell at various cycle numbers up to 200 cycles. The potential range was –0.03 to 1.12 V vs. SHE, and the current density was 1 A g^{-1} for both charge and discharge. c) The cycling performance of the CoCuHCF half-cell. The current density was 1 A g^{-1} for both charge and discharge. d) The rate capability of CoCuHCF.

continuous channel structure of CoCuHCF. The efficient Na ion diffusion was also reflected in the excellent rate capability. Even when tested at high C-rates of 10C, 20C, 40C, and 100C, specific capacities of 44, 43, 42, and 40 mAh g^{-1} were retained, respectively. The galvanostatic profiles at these C-rates are presented in Supporting Information Figure S7. Overall, the excellent electrochemical results position CoCuHCF as a promising SIB cathode material operating in neutral aqueous electrolytes.

With the motivation of developing more complete and practical energy storage platforms, (H)SNDI and CoCuHCF were integrated into full-cells (**Figure 5**a). The voltage profiles of (H)SNDI (red), CoCuHCF (blue), and full-cell (black) are comparatively presented in Figure 5b and Figure S8 (Supporting Information). The (H)SNDI/CoCuHCF full-cell showed average potential of ≈1.1 V, which is consistent with the voltage difference of both half-cells and is indeed quite ideal for aqueous batteries. The full-cell delivered 34 mAh g^{-1} at 20C charging/10C discharging when calculated based on the mass of CoCuHCF. It should be noted that although rechargeable batteries are usually measured in the conditions where charging is measured at a lower rate than discharging to simulate the discharging-limiting situations, we tested the cells in opposite conditions because the cycling performance (Supporting Information, Figure S9) measured at the same C-rates for charge and discharge turned out to be inferior to that of the given opposite condition. It is speculated that the inferior cycling performance on the same C-rates is ascribed to the fact that the desodiation process of SNDI is less kinetically efficient for Na ion diffusion than the sodiation process at high C-rates. In addition, the full-cell showed stable cycling performance (Figure 5c). At the aforementioned rate condition, 88% of the initial capacity was preserved after 100 cycles, and this robust cycling performance reconfirms the success of the cell integration. The cycling performance at lower C-rates was also investigated, and similar capacity retention was observed (Supporting Information, Figure S8). From the obtained full-cell results, we plotted a Ragone plot (Supporting Information, Figure S10) based on the weight of active materials on both sides. For reference, the energy density calculated based on the specific capacities obtained from the half-cell measurements using Equation S2 (Supporting Information) was 30 Wh kg^{-1}. In practice, we calculated the actual energy density based on ED = (total capacity measured) voltage/(mass of active materials on both electrodes), and the (H)SNDI/CoCuHCF full-cell showed an energy density of 26 Wh kg^{-1} at a power density of 53 W kg^{-1}, and 17 Wh kg^{-1} at 262 W kg^{-1}. As for the performance of the present hybrid aqueous cell, the energy densities are quite similar to those (15–27 Wh kg^{-1}) of the recent Prussian blue-based full-cells by the Cui group,[30] but is inferior to those of current commercialized LIBs, once again due to the use of aqueous media that restricts the operation voltage window and consequently electrode materials. As described above, the current case undergoes the additional sacrifice in the energy density owing to the neutral pH condition. Thus, the present hybrid battery compromises the energy density in the expense of the cost, safety, and environmentally friendly characteristic.

In summary, finding the appropriate electrode materials is the first critical step in the development of any new battery system. The two new active electrode materials investigated in the present study, (H)SNDI and CoCuHCF, demonstrated

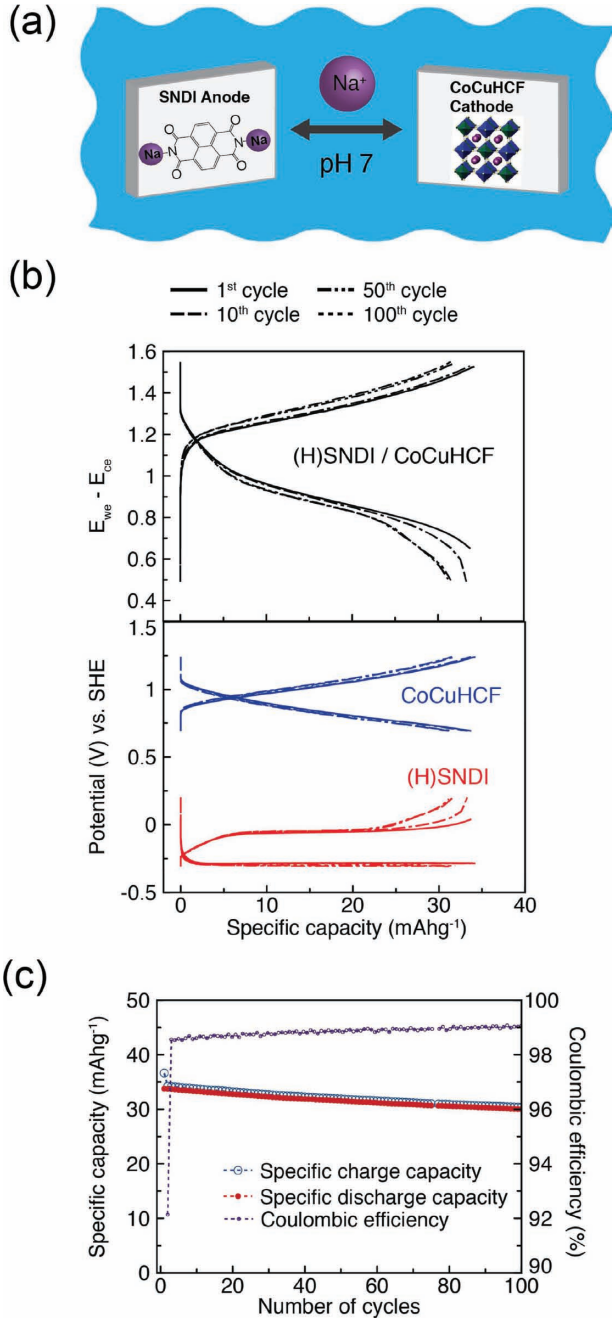

Figure 5. Electrochemical properties of the (H)SNDI /CoCuHCF aqueous full-cells. a) A schematic illustrating the full-cell configuration: cathode: CoCuHCF, anode: (H)SNDI. b) The galvanostatic profiles of the (H)SNDI/CoCuHCF full-cells as well as the isolated profile of each electrode from relative potentials against that of the reference electrode (SHE). c) The cycling performance and Coulombic efficiencies of the given full-cell.

excellent battery performance in both half-cell and full-cell settings even under the neutral aqueous electrolyte conditions. In particular, (H)SNDI and CoCuHCF exhibited redox voltages at the very low and high positions within the stable water potential window, enabling a high full-cell voltage of 1.1 V. By combining these two different classes of materials, we have introduced a hybrid aqueous full-battery concept, thus opening myriad of opportunities to develop more efficient integrated battery systems for large-scale battery applications. The current investigation delivers an important message that promising aqueous batteries for grid-scale ESSs could come to fruition by finding and optimizing previously uncommon battery materials.

Supporting Information

Supporting Information is available from the Wiley Online Library or from the author.

Acknowledgements

D.J.K. and Y.H.J. contributed equally to this work. The authors acknowledge financial support from the National Research Foundation of Korea (NRF) grant funded by the Korea government (MEST) (NRF-2010-C1AAA001–0029031 and NRF-2012-M1A2A2026587).

Received: January 22, 2014
Revised: March 9, 2014
Published online:

[1] J. M. Tarascon, *Philos. Trans. R. Soc. A* **2010**, *368*, 3227.
[2] B. Dunn, H. Kamath, J.-M. Tarascon, *Science* **2011**, *334*, 928.
[3] V. Palomares, P. Serras, I. Villaluenga, K. B. Hueso, J. Carretero-Gonzalez, T. Rojo, *Energy Environ. Sci.* **2012**, *5*, 5884.
[4] J. F. Whitacre, A. Tevar, S. Sharma, *Electrochem. Commun.* **2010**, *12*, 463.
[5] D. J. Kim, R. Ponraj, A. G. Kannan, H.-W. Lee, R. Fathi, R. Ruffo, C. M. Mari, D. K. Kim, *J. Power Sources* **2013**, *244*, 758.
[6] H. Qin, Z. P. Song, H. Zhan, Y. H. Zhou, *J. Power Sources* **2014**, *249*, 367.
[7] W. Li, J. R. Dahn, D. S. Wainwright, *Science* **1994**, *264*, 1115.
[8] R. Ruffo, C. Wessells, R. A. Huggins, Y. Cui, *Electrochem. Commun.* **2009**, *11*, 247.
[9] Z. Li, D. Young, K. Xiang, W. C. Carter, Y.-M. Chiang, *Adv. Energy Mater.* **2012**, *3*, 290.
[10] V. Palomares, M. Casas-Cabanas, E. Castillo-Martínez, M. H. Han, T. Rojo, *Energy Environ. Sci.* **2013**, *6*, 2312.
[11] K. Nakahara, K. Oyaizu, H. Nishide, *Chem. Lett.* **2011**, *40*, 222.
[12] Y. Liang, Z. Tao, J. Chen, *Adv. Energy Mater.* **2012**, *2*, 742.
[13] Y. Park, D.-S. Shin, S. H. Woo, N. S. Choi, K. H. Shin, S. M. Oh, K. T. Lee, S. Y. Hong, *Adv. Mater.* **2012**, *24*, 3562.
[14] Y. Kim, Y. Park, A. Choi, N.-S. Choi, J. Kim, J. Lee, J. H. Ryu, S. M. Oh, K. T. Lee, *Adv. Mater.* **2013**, *25*, 3045.
[15] S. Renault, D. Brandell, T. Gustafsson, K. Edström, *Chem. Commun.* **2013**, *49*, 1945.
[16] T. Nokami, T. Matsuo, Y. Inatomi, N. Hojo, T. Tsukagoshi, H. Yoshizawa, A. Shimizu, H. Kuramoto, K. Komae, H. Tsuyama, *J. Am. Chem. Soc.* **2012**, *134*, 19694.
[17] Y. Morita, S. Nishida, T. Murata, M. Moriguchi, A. Ueda, M. Satoh, K. Arifuku, K. Sato, T. Takui, *Nat. Mater.* **2011**, *10*, 947.
[18] D. J. Kim, S. H. Je, S. Sampath, J. W. Choi, A. Coskun, *RSC Adv.* **2012**, *2*, 7968.
[19] C. Sotiriou Leventis, Z. Mao, *J. Heterocycl. Chem.* **2000**, *37*, 1665.
[20] Z. Song, H. Zhan, Y. Zhou, *Angew. Chem. Int. Ed.* **2010**, *49*, 8444.
[21] M. Pasta, C. D. Wessells, R. A. Huggins, Y. Cui, *Nat. Commun.* **2012**, *3*. 1149
[22] E. Ahmed, G. Ren, F. S. Kim, E. C. Hollenbeck, S. A. Jenekhe, *Chem. Mater.* **2011**, *23*, 4563.

[23] S. Renault, J. Geng, F. Dolhem, P. Poizot, *Chem. Commun.* **2011**, *47*, 2414.
[24] Y. Liang, P. Zhang, J. Chen, *Chem. Sci.* **2013**, *4*, 1330.
[25] G. Andric, J. F. Boas, A. M. Bond, G. D. Fallon, K. P. Ghiggino, C. F. Hogan, J. A. Hutchison, M. A. P. Lee, S. J. Langford, J. R. Pilbrow, G. J. Troup, C. P. Woodward, *Aust. J. Chem.* **2004**, *57*, 1011.
[26] M. Armand, S. Grugeon, H. Vezin, S. Laruelle, P. Ribière, P. Poizot, J. M. Tarascon, *Nat. Mater.* **2009**, *8*, 120.
[27] C. D. Wessells, M. T. McDowell, S. V. Peddada, M. Pasta, R. A. Huggins, Y. Cui, *ACS Nano* **2012**, *6*, 1688.
[28] C. D. Wessells, S. V. Peddada, R. A. Huggins, Y. Cui, *Nano Lett.* **2011**, *11*, 5421.
[29] C. D. Wessells, R. A. Huggins, Y. Cui, *Nat. Commun.* **2011**, *2*, 550.
[30] M. Pasta, C. D. Wessells, N. Liu, J. Nelson, M. T. McDowell, R. A. Huggins, M. F. Toney, Y. Cui, *Nat. Commun.* **2014**, *5*, 3007.
[31] H. J. Buser, D. Schwarzenbach, W. Petter, A. Ludi, *Inorg. Chem.* **1977**, *16*, 2704.
[32] J. W. Mo, B. Ogorevc, X. Zhang, B. Pihlar, *Electroanalysis* **2000**, *12*, 48.